Analysis and Applications of Radiometeric Forces in Rarefied Gas Flows

Sergey F. Gimelshein*, Natalia E. Gimelshein*, Andrew D. Ketsdever† and Nathaniel P. Selden**

*ERC, Inc, Edwards AFB, CA 93524
† University of Colorado at Colorado Springs, Colorado Springs, CO 80933
**University of Southern California, Los Angeles, CA 90089

Abstract. An overview of recent numerical and computational studies of radiometric phenomena is presented. Several important factors affecting radiometric forces have been analyzed, including the contribution of area, edge, and shear forces for different pressures and gases, chamber size effect, gas-surface accommodation, and multi-vane geometries.

Keywords: Radiometric force, shear, ES-BGK equation
PACS: 51.10.+y

INTRODUCTION

Rarefied gas flow surrounding a thin vane with a temperature gradient imposed between its two sides exerts a force on the vane that tends to move it from the hot to the cold side. Such a force is conventionally called radiometric, as it is identified with the forces acting in the Crookes radiometer [1, 2] (although sometimes it is also called Knudsen force). There are three major components that contribute to the overall radiometric force on a vane. First, a pressure difference between the gas on the high temperature side and the low temperature side produces a net force. The molecules that reflect on the hot side have higher velocities than those reflected on the cold side, thus causing a force that acts from hot to cold. Since this force is acting on the entire area of the vane, it is called the area force hereafter. Second, there is an unbalanced force that exists near the edge of the vane, caused by the non-uniformity of the gas heating [3], henceforth called the edge force. Finally, thermal creep [2] in the form of a shear force acts along the lateral side of the radiometer in the direction from cold to hot.

A number of prominent scientists contributed to the current body of knowledge concerning radiometer flows toward the end of 19th and early 20th century [3, 4, 5]. The state of the art was summarized by Draper [6] as follows: (i) Maxwell's theoretical work showed that a temperature gradient must exist on the surface if tangential stresses are to arise; these stresses are the result of gas slipping over the surface from colder to hotter places. (ii) Einstein presented a simple account on how the length of the edge is important. (iii) Marsh and Loeb confirmed this experimentally. More recent studies of the origins of the radiometric force suggest that both Einstein's (edge) and Reynolds (shear) forces appear to contribute to the radiometric force, although it is still not clear which one is stronger.

Interest in these flows, while relatively low after 1920s, has seen a resurgence in the last decade, mostly related to the possibility of direct utilization of radiometric forces in many modern applications. One of the most important of these is atomic force microscopy (AFM), a research field that, although invented back in 1986 [7], has been brought to the forefront of modern nanotechnologies in the last several years. The use of radiometric forces as an approach to study gas-surface translational energy accommodation has been suggested by [8]. Gas flow around a laser opto-microengine was examined with the direct simulation Monte Carlo (DSMC) method [9]. This method was also used in [10], where the effect of the vane geometry on the radiometric force production was studied both numerically and experimentally. The solution of model kinetic equations has been applied to analyze the chamber size and gas pressure effects [11].

Unlike most of the present-day studies, this work does not concentrate on a specific device or application. Instead, it aims to establish the relative importance of three main mechanism that contribute to the overall radiometric force in flow regimes from free molecular to near continuum and analyzing various factors that generally impact the radiometric force in different flow conditions. The latter include the influence of facility effects, primarily proximity of chamber walls and chamber geometry, the importance of gas-surface interaction phenomena such as momentum and energy accommodation, the effects of radiometer vane geometry and, most importantly, the impact of holes in the vane.

EXPERIMENTAL SETUP

Four radiometer vane geometries were used in the experiments, and each consisted of a Teflon insulator placed between two aluminum plates. A resistive heater was located between one of the plates and the Teflon insulator, and the temperature of the hot side of the device was maintained by varying the power input to the heater. Each of the plates and the insulator are 0.32 cm thick, and when assembled yield an overall device thickness of 0.95 cm. The geometrical dimensions of the four vanes and the arm attachment setup are schematically shown in Fig. 1 (center). Each of these devices was individually mounted on a modified nano-Newton Thrust Stand (nNTS) [13] located inside a vacuum chamber. When calibrated using a set of electrostatic combs, the nNTS provides very accurate and repeatable data with typical force resolution of approximately 0.1μN and statistical scatter around 1%. Two vacuum chamber diameters were considered to study the effect of the walls, 0.4 m and 3 m. In the small chamber setup, a 0.4 m shell was placed into a large 3 m diameter vacuum chamber, as shown in Fig. 1 (right).

Experimental data was obtained for each device by evacuating the chamber to a base pressure below 10^{-4} Pa. A constant voltage was applied to the heater, which resulted in the main surfaces reaching temperatures of approximately 415 K (hot) and 360 K (cold). The background pressure inside the chamber was varied from 0.1 Pa to 6 Pa. Air, argon, helium, and xenon were utilized as test gases. Results presented are normalized by the temperature difference between the hot and the cold plates (ΔT) to account for small variations in the temperature. Verification of this normalization method has been conducted for temperature differences varying from 4 K to 30 K, and an exceptional linearity of the radiometric force with ΔT was observed [10].

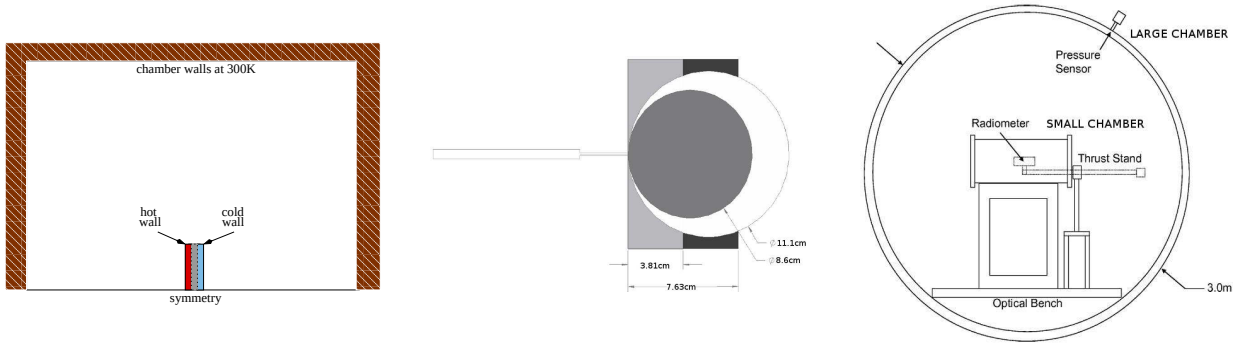

FIGURE 1. Left: computational setup. Center: vane geometries. Right: experimental setup (right).

COMPUTATIONAL TECHNIQUES

The numerical modeling of rarefied gas flow over a radiometer is conducted with two kinetic approaches, the DSMC method using SMILE computational tool [14], and a finite volume solution of the Ellipsoidal Statistical kinetic equation using SMOKE solver [15]. The use of a kinetic approach is complicated by significant computational cost, especially for the DSMC method, but it is necessary in order to account for rarefaction effects such as thermal stresses in the gas and thermal slip on the surface. In SMILE runs, the variable soft sphere model (VSS) with parameters listed in [16] was used for the molecular collisions, and the Maxwell model with full energy and momentum accommodation (except where specified otherwise) was used to calculate gas-surface collisions. SMOKE uses numerical schemes developed in [17]. A second order spatial discretization was used. The solutions were typically obtained in two successive steps. First, an implicit time integration scheme was run until the results converged. Second, an explicit time integration scheme was used with the initial conditions from the first step. This two-step approach allowed up to two orders of magnitude reduction in computational time compared to an explicit-only case. All results presented below are converged in terms of numbers of particles and cells (SMILE) and numbers of spatial cells and velocity bins (SMOKE). The error in the total radiometric force value is estimated to be typically less than 3% for DSMC runs (mostly due to statistical scatter) and less than 1% for ES runs (mostly due to the time convergence). The schematics of the computational setup are shown in Fig. 1 (left). Note that two temperature sets were used for the cold and hot sides of the radiometer, (1) 410 K and 450 K, and (2) 395 K and 420 K. The temperature of the insulator was assumed to be 430 K and 407 K, respectively. The chamber walls were always assumed to be 300 K.

RADIOMETRIC FORCE FOR DIFFERENT GASES

As mentioned above, the total radiometric force has three major components, area force, edge force, and shear force. In free molecular or nearly free molecular flows, only the area force is important. In this case, the momentum transfer between the gas and the vane is most efficient, and the radiometric force per unit pressure is highest. When gas pressure, and therefore collision frequency increases, the force per unit pressure decreases, since the collisions between reflected and incident particles effectively cut gas-vane momentum transfer. Further increase in pressure results in thermal transpiration flow, and the increase of relative importance of the edge and shear forces. In the near-continuum flow regime, however, the thermal nonequilibrium in gas becomes less significant, and the radiometric force essentially disappears. All this results in a bell-shape force versus pressure dependence (when pressure axis is in log scale), with a maximum force observed in the transitional regime. Such a bell-shape dependence was established experimentally as early as 1919 [19].

The radiometric force on a single-vane radiometer was measured and computed for different gases at different chamber pressures. Typical flow structure is shown in Fig. 2 (left) where the gas temperature is shown obtained by the two different solvers in 2D for temperature set (1) and a pressure of 1.2 Pa in a 0.4 m chamber. At this pressure, the radiometric force is near its maximum. There is a good agreement between the two solvers, with the temperature difference mostly not exceeding 1 K. Since the radiometer height (3.81 cm) based Knudsen number is about 0.1 (i.e. the flow is in the transitional regime), there is a noticeable temperature jump at the hot and cold sides of the radiometer, with the gas temperature being over 25 K lower than the corresponding radiometer wall temperatures. At the chamber walls, the gas temperature is about 300 K. The streamlines manifest some statistical scatter in the DSMC solution, but are qualitatively similar to the ES result. There are four vortices formed in the chamber, two at each side of the vane. The vortices at the hot side are much stronger than those at the cold side; the maximum bulk flow velocities approach 1 m/s. Note that such a four-vortex structure is qualitatively different from a two-vortex flow pattern that is conventionally attributed to radiometric flows (illustrated in [18]). In detailed ES simulations (not shown here), the four-vortex flow was found to transform to two-vortex at significantly lower Knudsen numbers (less than 0.01), where the thermal transpiration from cold to hot starts to dominate the bulk flow motion.

The dependence of the total radiometric force on gas pressure for different gases (nitrogen, helium, and argon) computed with the DSMC method for temperature set (1) in a 0.4 m chamber is shown in Fig 2 (center). As expected, all gases produce nearly identical force in the free molecular regime. The force maximum is observed at a Knudsen number of about 0.1 for all three gases. The largest force is observed for helium, since its mean free path for a given pressure is maximum, and thus the impact of the area (free molecular) force propagates further in pressure than for the other two gases. It is interesting to note that the the radiometric force for nitrogen is somewhat smaller than that for argon, even though the mean free path is larger in nitrogen. The reason for this is believed to be the internal degrees of freedom that decrease the gas-vane momentum transfer. The impact of the internal modes of molecules on the radiometric force was first noted in [20] where the force decrease for molecular gases was analytically evaluated.

The experimental measurements provide qualitatively similar results for the three gases considered in the computations, as shown in Fig. 2 (right). Helium is characterized by the maximum radiometric force, although for intermediate pressures the force in helium is smaller that that for other gases due to incomplete gas-surface accommodation as will be shown below. The force in argon is larger than that in nitrogen, and two heavier gases (CO_2 and Xe) produce even smaller forces.

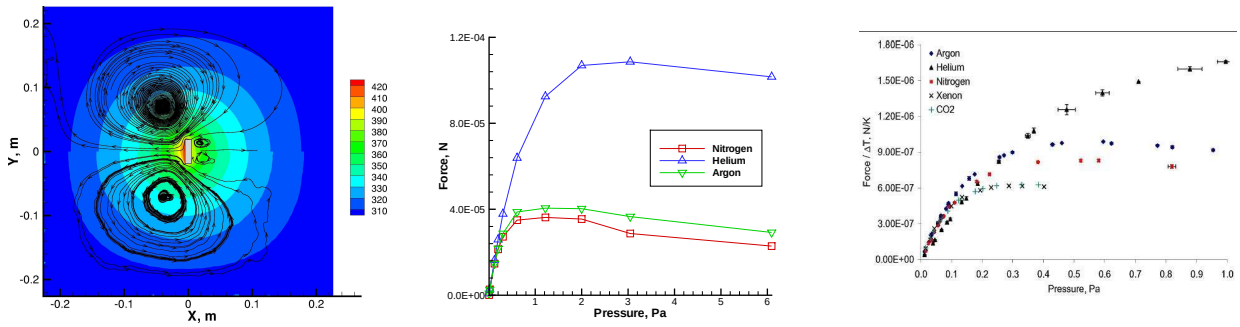

FIGURE 2. Left: temperature fields and streamlines in argon obtained with SMOKE, top, and SMILE, bottom. Center: radiometric force for different gases obtained with SMILE. Right: measured force for different gases.

AREA, EDGE, AND SHEAR FORCE CONTRIBUTION

It is clear from simple kinetic theory considerations that when the gas collision frequency is low, the area force is the main contributor to the radiometric force. For high collision frequencies, as was pointed out by Reynolds, molecules with higher velocities leave the hot side of the vane and collide with incoming molecules, reducing the surface flux more efficiently than the collisions of molecules reflected on the cold surface. Essentially, this means that these effects compensate each other, and the values of gas pressures in the center of the vane become equal at the hot and cold sides. Near the edges of the vane, there is still an unbalanced force that drives the radiometer at higher pressures. This is illustrated in Fig. 3 (left) where the gas pressure in argon at 1.2 Pa (where the total force is maximum) is shown, as calculated with the ES approach for temperature set (1) in the small 2D domain. Only a small part of the domain is presented to provide more detail in the vicinity of the vane. It is clearly that the pressure is maximum near the edges of the cold and hot sides; it is also high near the lateral side of the vane.

Not only is the absolute pressure maximum near the edges, but the pressure difference between the hot and the cold sides is also a maximum. This is seen in Fig. 3 (center) where the difference between surface pressures on the hot and cold sides is given for argon at four chamber pressures. This figure also illustrates the relative contribution of area and edge forces. At the lowest gas pressure (Kn≈0.5), the pressure difference is nearly uniform along the plate, which indicates that the area forces are dominant. At the highest gas pressure, the surface pressures at the center of the vane are equal at the cold and hot sides, and only the edge force is important. The quantitative analysis of the area and edge force contribution may be conducted through comparison of forces for two different vane sizes. Figure 3 (right) shows the radiometric forces, normalized by the vane temperature difference, for a small and a large vane. Their area ratio is 0.5, while the perimeter ratio is 1 due to the flow two-dimensionality. If only area forces were important, the small-to-large force ratio would be equal to 0.5, while if only edge forces were important, the small and large plate forces would be equal. In the region of pressures where the force is maximum, the small-to-large vane force ratio is about 0.7, which indicates that both area and edge forces contribute to the total force.

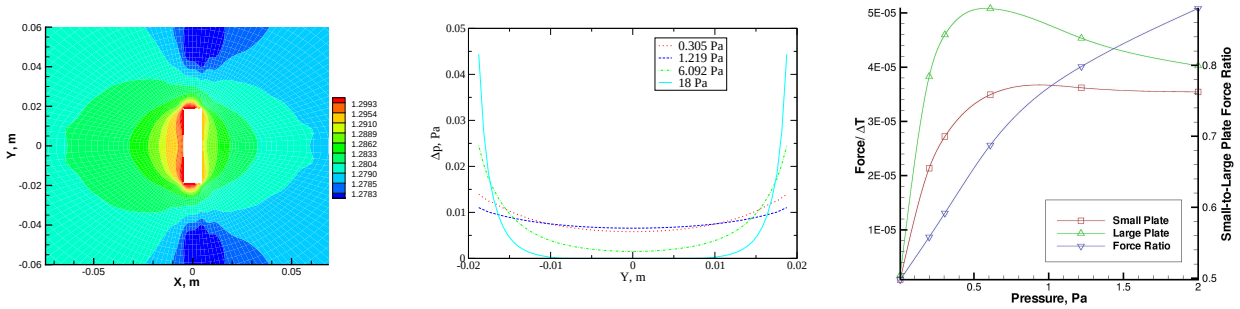

FIGURE 3. Left: pressure fields at 1.2 Pa. Center: surface pressure difference between hot and cold sides. Right: radiometric force for two vane sizes. Argon gas, ES approach, 2D.

Similar conclusion may be drawn from the experimental results presented in Fig. 4 (left, center). The results show that the forces on the rectangular and large circular plate are very close, while that on the smaller circular plate is systematically lower. From Fig. 4 (center), where the results are shown as force ratios, it is seen that in the low pressure region the force is proportional to the plate area. This is consistent with predictions made by free molecular theory. As the flow transitions from the collisionless regime, the picture becomes distinctly more complex. While it is readily observed that the plates with larger area produce more force at their respective peaks, the force-to-area ratio does not hold. When comparing the peaks of the large and small circular plates, it is found that small plate creates 72% of the force of the larger one. Similarly to the numerical prediction, this is between the area ratio (60%) and the perimeter ratio (77%). The general conclusion may be drawn that both area and edge forces are important in the range of pressures where the radiometric force is near its maximum. As for the shear force on the lateral side of the vane, the numerical analysis shows that its contribution is negligibly small for small pressures and increases for pressures to the right of those where the peak force is observed. This is illustrated in Fig. 4 (right). Note that in all cases the shear force reduces the total force.

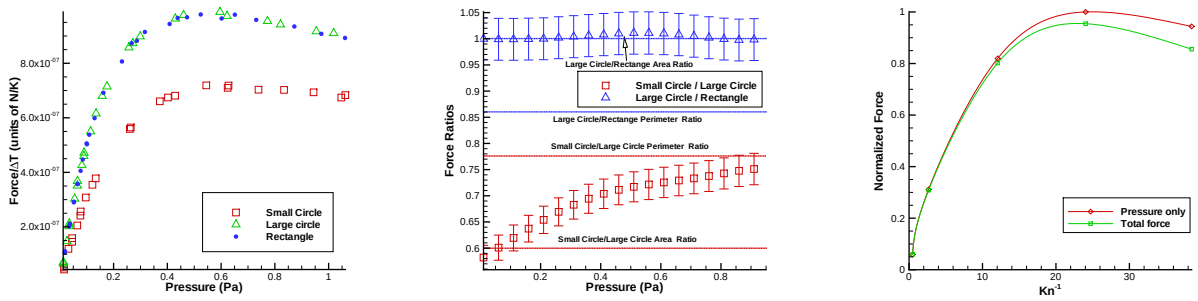

FIGURE 4. Left: Measured force on three different plates in argon. Center: Comparison of measured force ratios for two geometry pairs. Right: total radiometric force and no-shear (pressure only) force computed in axisymmetric small domain.

RADIOMETRIC FORCE ESTIMATE

For free molecular flow, there is an exact expression for the radiometric force on the vane, expressed as

$$F = \frac{p}{2} A \left(\sqrt{\frac{\alpha_E T_h + (1-\alpha_E) T_g}{T_g}} - \sqrt{\frac{\alpha_E T_c + (1-\alpha_E) T_g}{T_g}} \right), \tag{1}$$

where T_h and T_c are the hot and the cold side temperatures, respectively, T_g is the free stream gas temperature, A is the area of the vane, and α_E is the energy accommodation coefficient. For collisional flow, some assumptions have to be used in order to obtain an approximate analytic expression. One of the earlier derivations was presented in Ref. [21], whose authors started from a rigorous theory proposed in Ref. [3]. This theory described a phenomenon, later called thermal transpiration, where fluid particles move from the cold side of the vane to the hot side, with the reaction to this flow current being a force on the vane towards the cold side. The region where this force is observed is therefore the lateral sides of the vane, and the force per unit area is [21] $F = \frac{3}{4} \frac{\eta^2}{a\rho T} \frac{\partial T}{\partial x}$, where η is the coefficient of viscosity, ρ is the density, a is the distance to the opposite vane (or, generally, to the chamber walls), T is the temperature, and x is the length along the axis chosen parallel to the temperature gradient.

Another theory [5] is also based on some elements of the thermal transpiration phenomenon, although the radiometric force is assumed to be produced on the main side of the plate in an area that is one mean free path thick. The force is acting on the vane perimeter and is given per unit length of the edge as $F = p\lambda \frac{\Delta T}{T}$, where p is gas pressure, λ is the gas mean free path, ΔT is the temperature difference, and T is the absolute temperature. This theory found partial confirmation in the experiments [22]. Later, Sexl [20] showed that Einstein's theory was deduced from a reasoning which was not strictly accurate, and he modified the theory and derived an expression for the radiometric force on a dish radiometer [see 20] as $F = \frac{14.72}{n+5} \frac{p\lambda^2}{T} \Delta T$, where n is the number of active internal degrees of freedom of gas molecules (0 for a monatomic gas). The main difference between Sexl and Einstein's formulas is that Sexl's radiometric force is inversely proportional to gas pressure while Einstein's force is independent of pressure and is proportional to the perimeter of the vane.

Most recently, a new expression for radiometric force was derived [23], that has both pressure F_n and shear F_τ components,

$$F_n = (2-\alpha_E) \frac{15k}{32\sqrt{2}\pi\sigma^2} \Delta T l, \; F_\tau = \alpha_E \frac{15k}{64\sqrt{2}\pi\sigma^2} \frac{\Delta T}{\lambda} (\tau l),$$

where α_E is the energy accommodation coefficient, k is the Boltzmann constant, $\pi\sigma^2$ is the total collision cross section, l is the vane perimeter, and where τ is the vane thickness.

For many radiometric devices, the maximum force is observed at a Knudsen number about 0.1. For flows at Knudsen numbers close to this value, the contribution of the edge forces is expected to be fairly large, and comparable to that of the area forces [10]. Obviously, with the increase of gas pressure and decrease in the Knudsen number the surface area where the edge-related radiometric force is significant will decrease, since it is proportional to the gas mean free path. Therefore, an effective area may be introduced for a circular vane as

$$A = \pi \mathbf{R}_{eff}^2 = \pi \mathbf{R}^2 - \pi (\mathbf{R} - n\lambda)^2, \tag{2}$$

where **R** is the vane radius, λ is the mean free path of the ambient gas, and $n\lambda$ specifies the thickness of the edge area where the force is produced. This effective area, when plugged into the free molecular expression (1), may be used for an evaluation of the radiometric force. Note that in the limit of $\lambda \to 0$ the force predicted with this expression becomes independent of pressure, similar to [5]. If an assumption similar to [5] is made and $n = 1$ is used, the radiometric force computed with a simple empirical expression Eqs. (1)-(2) gives surprisingly close agreement with the present experimental results ([10]), as shown in Fig. 5 (left). It is interesting to note that the assumption of $n = 1$ works very well, even though it has been shown above that the pressure imbalance occurs over a region of at least ten mean free paths.

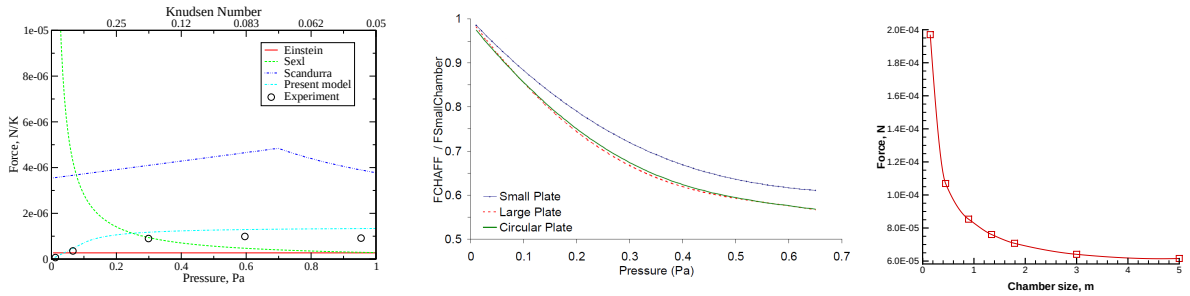

FIGURE 5. Left: analytic estimates of radiometric force in argon as compared to the data. Center: measured large chamber to small chamber force ratio for different vane geometries. Right: chamber size dependence of radiometric force modeled with DSMC.

CHAMBER SIZE EFFECT

The proximity of the walls of the chamber where the radiometric vane is located is expected to influence the resulting radiometric force. The only exception is for free molecular flow with fully diffuse surface accommodation, where the force is independent of chamber geometry and size. Such a dependence on the chamber walls was recognized as early as 1920s [21], when the radiometric force was predicted to be inversely proportional to the distance between the radiometer plane and the chamber walls. In order to study the quantitative dependence of the radiometric force on the chamber size, measurements were performed with three different vane geometries in two chambers, a small 0.4 m diameter chamber and a large 3 m diameter chamber. Note that in both chambers, the radiometer vane was placed in the chamber center to avoid preferential impact of the walls on the cold or hot sides of the vane. The results are summarized in Fig. 5 (center) where the ratio of radiometric forces obtained in large chamber to those in small chamber is presented for argon gas. For low pressures, where the flow approaches the free molecular limit, the force ratio tends to unity since the argon atoms reflect nearly diffusely on stainless steel surfaces of the chambers.

As the gas pressure increases, the force ratio decreases, which clearly indicates that the proximity of the chamber walls increases the total force. The main reason for this is that temperature gradients become steeper for the small chamber, thus increasing the net momentum flux to the vane. The decrease in the force ratio is nearly identical for the large rectangular plate and circular plate that have the same areas. However, the small rectangular plate is characterized by smaller influence of the chamber size. This indicates that not just the distance between the hot and cold sides and the chamber walls are important, but also the chamber volume to the plate area ratio. The facility impact is smaller for larger volume-to-area ratios. The computations have shown similar trend of decreasing the radiometric force with increasing chamber size, as shown in Fig. 5 (right), where the force as a function of chamber size is given for a 2D argon flow over a small plate at 0.3 Pa computed with the ES method (temperature set 1). For 2D flow, the chamber size needs to be about two orders of magnitude larger than the vane size in order to minimize the chamber wall effect. Note that for axially symmetric flow, a 1.5 m chamber is sufficient for the facility effects to be negligibly small.

RADIOMETRIC FORCE AND GAS-SURFACE ACCOMMODATION

When the chamber is large enough, and its effects are negligible, the radiometric force on the vane is governed by collisions of gas molecules with the vane surface. In free molecular flow, the force dependence on pressure is known, and for given vane temperatures it is a function of the surface accommodation only. The accommodation

coefficients may therefore be found easily if such a free molecular force is measured experimentally. However, the current capabilities do not allow for measurements of radiometric force in free molecular regime with acceptable accuracy of 1-2%. In order to obtain accommodation coefficients, it is therefore necessary to measure the force in the transitional regime, and then compare it to the corresponding numerical predictions [11]. DSMC computations of radiometric flows in large chambers are computationally impractical, while ES results in small chambers were found to underpredict the DSMC results by about 10% in the range of pressures where the force is near its maximum. An approach was therefore developed [24] that combined the ES modeling of a large domain bounded by chamber walls with the successive DSMC modeling of a much smaller domain surrounding the vane, with the boundary conditions provided from the ES computation (ellipsoidal distribution of incoming molecules in DSMC is based on ES macroparameters calculated from the inflow gas properties). The results for argon flow in a small chamber are given in Fig. 6 (left) and illustrate the accuracy of the combined ES/DSMC approach. Note that the error bars are estimated to be about 1% for ES simulations and about 3% for ES/DSMC.

This approach was first used for helium flow over a large circular vane in the large chamber. Comparison of numerical and experimental results is presented in Fig. 6 (center). Here, the results of the computations using the combined ES/DSMC approach are shown for the fully diffuse reflection (closed symbols) and the Maxwell model with the momentum accommodation coefficient of 0.5. It is seen that the fully diffuse model largely overpredicts the data, with the numerical points being about two times larger than the corresponding experimental values. However, the results for $\alpha = 0.5$ are very close. Therefore, it may be concluded that the helium atoms accommodation on engineering surfaces of aluminum is incomplete, with the accommodation coefficient close to 0.5. The ratio of calculated with $\alpha = 1$ to measured radiometric forces for three noble gases is given in Fig. 6 (right). It is interesting to note that there is no obvious dependence of this ratio on gas pressure, and all points for a given gas are within the error bar of the experiments and computations. The dashed lines show the average values of the ratios. The ES/DSMC computations conducted with the corresponding values of α have shown that the best fit to the data provide α of 0.53 for helium, 0.81 for argon, and 0.86 for xenon. Those values agree reasonably with those available in the literature [25], which validates the radiometric approach to obtain accommodation coefficients.

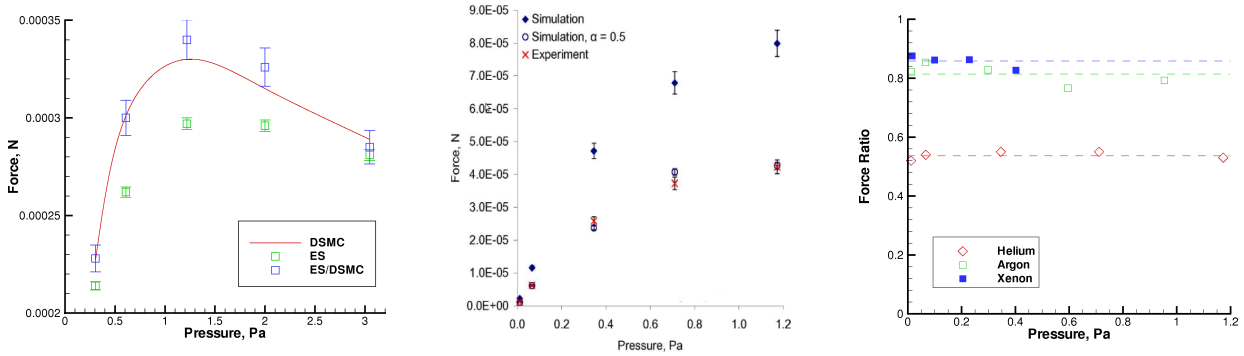

FIGURE 6. Left: comparison of forces on a small vane in argon obtained with three different approaches. Center: comparison of measured and computed forces in helium for two accommodation coefficients. Right: experimental to computed force ratios for three gases at different pressures.

MULTI-VANE GEOMETRIES

It has been shown above that both area and edge forces contribute to the total radiometric force, usually peaking at vane-length based Knudsen numbers of about 0.1. Decreasing the vane size would generally shift the force maximum to higher pressures, effectively increasing the force per unit length of the vane. The important question arises related to the possibility of increasing the total radiometric force per unit length through etching holes in a single vane. It would now represent a large number of smaller vanes that occupy the same total area. 2D computations have been conducted with the ES method to study the effect of the hole dimensions (or, in other words, small vane separation), and the total number of smaller vanes (or the small vane size). The schematics of the computational setup are shown in Fig. 7 (left) where the multi-vane and single vane geometries are compared. Note that a relatively small chamber size was used to make the computations more efficient. Comparison of results for multi-vane geometries where the total radiometer area does not change, all vane sizes are equal, and only the number of vanes varies, allowed the optimum

separation between the vanes (in terms of force per total vane length or radiometer mass) to be found, as illustrated in Fig. 7 (center). Note that maximum forces are presented here, which typically occurred at a Knudsen of about 0.03 based on the small vane length. It is seen that a separation of about 70% of the vane length represents the optimum configuration. With the separation fixed to 70% of the small vane length, the number of vanes was then increased in order to analyze the potential impact of etching a large number of holes in a single vane. The gas pressure was also varied to find the maximum force for a given geometry. The resulting maximum forces are presented in Fig. 7 (right) for two chamber sizes. The main conclusion here is that etching holes allows for significant increase in the total radiometric force, although further increase is hampered by increasing shear forces. Note that force increase is expected to be even more significant when a 3D geometry (and square vanes) is used.

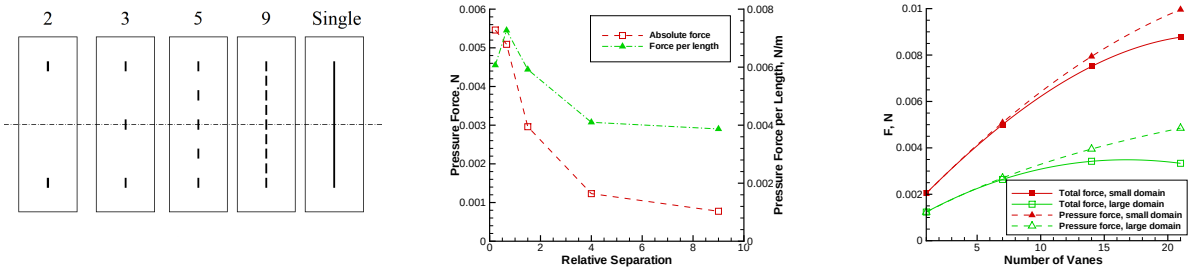

FIGURE 7. Left: multi-vane computational setup. Center: impact of vane separation on total force. Right: force increase in multi-vane geometries.

Acknowledgements. The work was supported in part by the Propulsion Directorate of the Air Force Research Laboratory at Edwards Air Force Base California. The authors thank Phil Muntz, Ingrid Wysong, Dean Wadsworth, and Alina Alexeenko for many fruitful discussions.

REFERENCES

1. W. Crookes *Philosophycal Transactions of the Royal Society of London.* (1874) **164**, 501–527.
2. L.B. Loeb, *The kinetic theory of gases.* Dover Publications Inc., (1961) 364–386.
3. J.C. Maxwell, *Phil. Trans. R. Soc. of London* **170** (1879) 231-256.
4. O. Reynolds, *Phil. Trans. R. Soc. of London* **170** (1879) 727-845.
5. A. Einstein, *Zeitschrift fur Physik* **27** (1924) 1-5.
6. C. W. Draper, J. Chem. Education, **53**(6), 357 (1976)
7. G. Binning, C.F. Quate, C.H. Gerber, *Physical Review Letters*. **56** (1986) 930–933.
8. A. Passian, R.J. Warmack, T.L. Ferrell, T. Thundat, *Phys. Rev. Lett.* **90** (12) (2003) 124503.
9. M. Ota, T. Nakao, M. Sakamoto, *Math. and Computers in Simulation* **55** (2001) 223-230.
10. N. Selden, C. Ngalande, S. Gimelshein, E.P. Muntz, A. Alexeenko, A. Ketsdever, *Phys. Rev. E* **79** (2009) 041201.
11. N. Selden, N. Gimelshein, S. Gimelshein, A. Ketsdever, *Phys. Fluids* **21**(7) (2009) 073101.
12. G. Benford, J. Benford, *Acta Austonautica* **56** (2005) 529-535.
13. A.J. Jamison, A.D. Ketsdever, and E.P. Muntz, *Review of Scientific Instruments* **73**, 3629 (2002)
14. M.S. Ivanov, S.F. Gimelshein, G.N. Markelov, *Computers and Mathematics with Applications* **35**(1-2) 113 (1998)
15. N. Selden, C. Ngalande, N. Gimelshein, S. Gimelshein and A. Ketsdever, *Journal of Fluid Mechanics* **634** (2009) 419-431.
16. G. A. Bird, *Molecular Gas Dynamics and the Direct Simulation of Gas Flows*, Clarendon Press, Oxford, 1994.
17. L. Mieussens, *J. Comp. Phys.* **162** 429-466 (2000).
18. E.H. Kennard, *Kinetic theory of gases*, McGraw-Hill, New York (1938)
19. W. H. Westphal, *Zeit. fur Physik* **1** 92 (1920)
20. Th. Sexl, *Annalen der physik* **81**(24) 800–806 (1926).
21. G. Hettner and M. Czerny, *Zeitschrift fur Physik* **30** 258–267 (1924).
22. H.E. Marsh, *Journal of Optical Society of America* **12** 135–148 (1926).
23. M. Scandurra, F. Iacopetti, and P. Colona, *Physical Review E* **75** 026308 (2007).
24. N. Gimelshein, S. Gimelshein, N. Selden, A. Ketsdever, Accepted to *Vacuum*, 2010.
25. W. M. Trott, D. J. Rader, J. N. Castañeda, J. R. Torczynski, M. A. Gallis, *Proc. XXVI Int. Symposium on Rarefied Gas Dynamics*, Kyoto, Japan, July 2008.